JOURNAL OF GEOPHYSICAL RESEARCH, VOL. 89, NO. A12, PAGES 10,813–10,826, DECEMBER 1, 1984

Nonlinear Pitch Angle Scattering and Trapping of Energetic Particles During Landau Resonance Interactions With Whistler Mode Waves

S. TKALCEVIC, U. S. INAN, AND R. A. HELLIWELL

Space, Telecommunications, and Radioscience Laboratory, Stanford University, California

The time averaged equations of motion derived by Inan and Tkalcevic (1982) are used in a test particle study of Landau resonant interactions of whistler mode waves and energetic particles in the magnetopshere. By computing individual particle trajectories it is shown that the pitch angle scattering and energy exchange is significantly different for the two classes of particles, trapped and untrapped. The trapped particles are characterized by a bounded phase variation, whereas the nontrapped particles exhibit unbounded phase variation. The threshold wave electric field intensities necessary for trapping are determined. Full distribution test particle simulation is carried out to determine the precipitated electron flux that would be induced as a result of these interactions. It is shown that for typical parameters the resulting precipitation fluxes for Landau resonance interactions are much smaller than those induced in gyroresonance interactions, even for wave field intensities that are much higher than the trapping threshold.

1. INTRODUCTION

It is known that very low frequency waves can propagate in the magnetosphere in the whistler mode with phase velocities much smaller than the velocity of light. Such waves can undergo interactions with energetic particles both through longitudinal (Landau) resonance and cyclotron (gyro) resonance. In longitudinal resonance the particle parallel velocity is matched to the wave phase velocity, whereas in the cyclotron resonance the doppler-shifted frequency of the wave (shifted due to the particle parallel velocity) matches the gyrofrequency of the energetic particle. Both types of interactions may induce perturbations of the energetic particle distribution through pitch angle scattering and may also result in different types of radio wave emissions, wave amplification (growth), and wave attenuation. The purpose of this paper is to investigate the nonlinear longitudinal resonance interactions of energetic particles with whistler mode signals propagating at an oblique angle to the static magnetic field.

Longitudinal (or Landau) resonance interactions between waves and energetic particles have been invoked to explain auroral VLF hiss [*Jorgensen*, 1968; *Swift and Kan*, 1975; *Maggs*, 1976]. Landau resonance with energetic electrons may also play an indirect role in the generation of other waves. For example, *Thorne et al.* [1973] have attributed the observed sharp lower-frequency cutoff of plasmaspheric hiss to Landau damping of oblique whistler waves by electrons.

Landau resonance interaction was invoked in the context of a proposed mechanism for whistler precursors [*Park and Helliwell*, 1977]; it was suggested that the triggering of the precursor via gyroresonance was facilitated by a temporary enhancement of equatorial density of energetic particles resulting from their having been previously trapped by the whistler through Landau resonance. More recently, bursts of electrostatic noise that occur in association with whistler mode chorus emissions have also been attributed to generation by beams of electrons trapped in Landau resonance with the chorus [*Reinleitner et al.*, 1982, 1983]. Observations of similar types of chorus-related electrostatic bursts in the Jovian and Saturnian magnetospheres have demonstrated that coupling between longitudinal and cyclotron resonance interactions may be of importance in planetary magnetospheres [*Reinleitner et al.*, 1984].

While some generalized computer simulation studies of the longitudinal resonance interaction have been made [*Cuperman and Sternlieb*, 1974], the detailed nonlinear motion of Landau resonant particles has been reported only for electrostatic waves [*Nunn*, 1971 1973]. For interactions involving obliquely propagating whistler mode waves a new set of nonlinear equations of motion was recently derived by time averaging the wave forces over one cyclotron period and were shown to describe accurately the particle motion for most magnetospheric parameters of interest [*Inan and Tkalcevic*, 1982]. These equations are particularly suited for test particle simulation and are utilized in the analysis reported here.

The approach we adopt is to use the computed nonlinear trajectories of distributions of test particles for studying the dependence of the resonance process on various parameters and phenomena such as wave growth and damping, particle trapping and wave-induced pitch angle scattering. In the following, we first briefly describe the nonlinear equations of motion used in computing particle trajectories. We then describe the model used and investigate the scattering and trapping of selected test particles. This is followed by a full distribution analysis presented in section 5.

2. EQUATIONS OF MOTION

The equations of motion are derived by considering the general Lorentz force equation governing the interaction of an electron with an elliptically polarized wave propagating in the magnetosphere,

$$m d\mathbf{v}/dt = q[\mathbf{E}_w + \mathbf{v} \times (\mathbf{B}_w + \mathbf{B}_o)] \quad (1)$$

Paper number 4A8052.
0148-0227/84/004A-8052$05.00

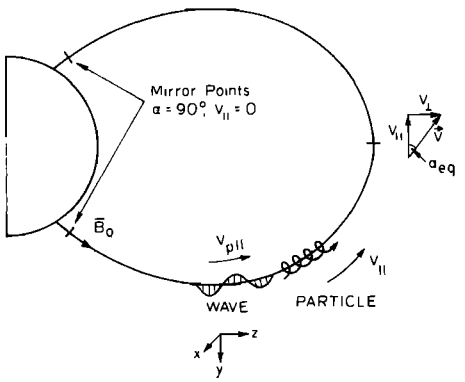

Fig. 1. Dipole geometry and symbols used for particle identification. Note that the z-axis is aligned with the magnetic field line and that both the wave and the particles travel in the $+z$ direction. Particle orbits are described in terms of equatorial values of $v_{\|}$ and α.

which when averaged over one gyroperiod gives the nonlinear set of equations first derived by *Inan and Tkalcevic* [1982] as

$$\frac{dv_{\|}}{dt} = \frac{q}{m}E_z J_0(\eta)\left[1 - \frac{v_\perp k\cos\theta}{\omega}\rho_z\frac{J_1(\eta)}{J_0(\eta)}\right] \sin(\omega t - kz\cos\theta) - \frac{v_\perp^2}{2\omega_H}\frac{d\omega_H}{dz} \tag{2}$$

$$\frac{dv_\perp}{dt} = -\frac{q}{m}\rho_z E_z J_1(\eta)\left[1 - \frac{v_{\|}k\cos\theta}{\omega}\right] \sin(\omega t - kz\cos\theta) + \frac{v_{\|}v_\perp}{2\omega_H}\frac{d\omega_H}{dz} \tag{3}$$

where J_0 and J_1 are the Bessel functions of the first kind and zero and first order respectively, ω_H is the electron gyrofrequency, k is the wave number, ω is the wave frequency, q and m are the electronic charge and mass, respectively, θ is the wave normal angle, $E_z(E_{\|})$ is the wave electric field component parallel to $\mathbf{B}_o$, ρ_z is the wave longitudinal polarization ($\rho_z = iE_y/E_z$), and other quantities and the coordinate system are as shown in Figure 1.

The quantity η is defined [*Inan and Tkalcevic*, 1982] as

$$\eta = \frac{\omega}{\omega_H}\tan\theta\tan\alpha \tag{4}$$

where $\alpha = \tan^{-1} v_\perp/v_{\|}$ is the particle pitch angle.

In (2) and (3) the $J_1(\eta)$ terms represent the effects of the wave magnetic field components ($q\mathbf{v}\times\mathbf{B}_\omega$) and the $J_0(\eta)$ term represents the fact that the E_z field seen by the particle in the course of a gyroperiod is not uniform since E_z has transverse phase variation in addition to phase variation along z. The averaging of (1) over one gyroperiod is only valid if

$$\omega - \mathbf{k}\cdot\mathbf{v} \ll \omega_H \tag{5}$$

which is clearly the case for particles near Landau resonance with the wave, where the left-hand side of (5) is approximately zero.

The magnitude of the various terms in (2) and (3) were examined as a function of wave normal angle, particle pitch angle, and wave frequency, and it was concluded that the $J_1(\eta)$ terms can be neglected under conditions of low pitch angles, high wave normal angles, and/or high normalized wave frequencies (ω/ω_H). In such cases the wave-particle interaction is similar to that involving an electrostatic wave having only a E_z component [*Inan and Tkalcevic*, 1982].

In the following analysis we use the complete equations (2) and (3) for computing trajectories of test particles near Landau resonance with obliquely propagating whistler mode waves. It should be noted that these equations are nonlinear, i.e., they account for wave-induced changes of the particle velocity components $v_{\|}$ and $v_\perp$. Thus nonlinear phenomena such as trapping of particles in the wave's potential well, can be conveniently described by these equations. Even though the equations are obtained by averaging over one gyroperiod, they are indeed quite accurate for the description of particle motion since (5) is satisfied at all times for near-Landau resonant particles. Because of the averaging, the resultant equations are particularly suitable for computer simulation, since they allow the use of integration time steps much coarser than a gyroperiod, a significant saving in computation time. In this respect the test particle study presented here is different from that carried out by *Reinleitner et al.* [1983]. These authors studied particle trapping in a homogeneous medium using periodic boundary conditions and selected test particles. Also since they did not employ the time averaged equations (2) and (3), they had to use time steps that are as small as one twentieth of the electron cyclotron period. Our formulation, because of the large saving in computer time with little loss in accuracy [*Inan and Tkalcevic*, 1982], lends itself to the treatment of the full interaction in an inhomogeneous medium using a full distribution of particles.

3. Description of Model

In using (2) and (3) for the determination of the test particle trajectories we consider the case of an elliptically polarized whistler mode signal of constant amplitude $E_{\|}(E_z)$ propagating at a constant angle θ with respect to the static magnetic field (i.e., $\mathbf{k} \parallel \mathbf{B}_o$). In other words, both the wave intensity $E_{\|}$ and wave normal angle θ seen by the particles as they move along the field line are assumed constant. It should be noted here that this is a simplifying assumption since for typical non-field-aligned whistler mode propagation in the magnetosphere, both of these quantities, as seen by a particle confined to a given field line, would be expected to vary. To treat the general case, ray-tracing analysis in a model magnetosphere must be carried out in order to determine the variation of θ as well as signal intensity as would be obtained from the focusing/defocusing of the rays and the local refractive index. While such an analysis is straightforward in principle, the results (i.e., the ray path distribution) are dependent on the background magnetospheric cold plasma density variation, which itself is variable. Thus it is difficult to select a typical set of conditions. A ray path distribution with approximately constant nonzero wave normal angle θ along the magnetic field may result under some conditions. An example is propagation with $\theta = \theta_g$, where θ_g is the Gendrin angle [*Gendrin*, 1961]. In this case, waves can be guided in field-aligned density depressions [*Inan and Bell*, 1977]. We submit therefore that our assumption is justified, especially in view of our purpose in this paper, namely, to describe quantitatively the physics of the nonlinear resonant interaction, to determine the conditions for trapping, and to estimate the precipitated flux.

Note that except for the assumptions cited above, our

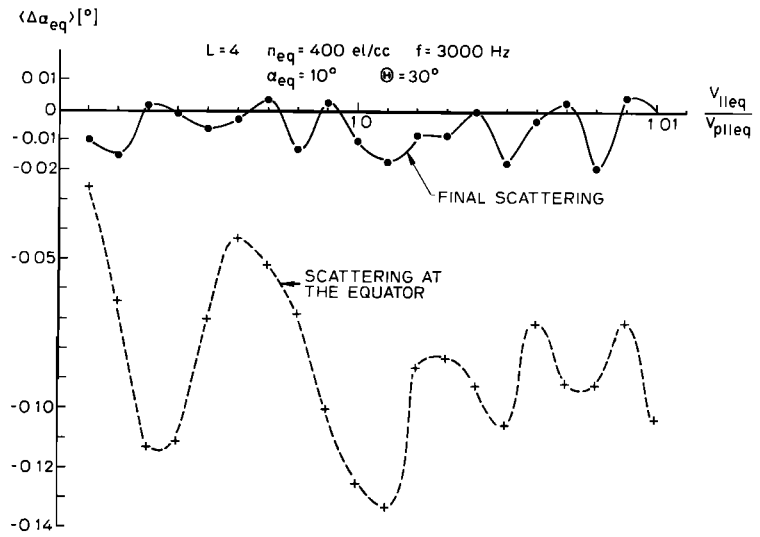

Fig. 2. Mean scattering as a function of parallel velocity. Electrons interacting with a CW signal exhibit a small final scattering (solid curve), whereas the cumulative scattering evaluated at the equator is significantly larger (dashed curve).

treatment accounts for the inhomogeneity of the medium in that the quantities ρ_z, ω_H, and k in (2) and (3) are treated as functions of z. The cold plasma density along the magnetic field lines is assumed to be governed by diffusive equilibrium [*Angerami and Thomas*, 1964], while for the variation of the earth's magnetic field we use a centered dipole model.

The particle populations are represented by "sheets" of particles initially uniformly distributed in phase (relative with respect to the wave) but all having the same equatorial parallel velocity ($v_{\|_{eq}}$) and pitch angle (α_{eq}). In the following we study the pitch angle scattering and nonlinear trapping of such individual sheets of particles in sections 3 and 4. We then consider many such sheets, distributed appropriately in $v_{\|_{eq}}$ and α_{eq}, to represent a full distribution of particles in section 5.

4. Scattering of a Single Sheet of Particles

For any given initial $v_{\|_{eq}}$ and α_{eq}, we consider in our simulation 12 test particles initially distributed uniformly in phase with respect to the wave. For each of these particles the equations of motion (equations (2) and (3)) are integrated over the portion of the field line where the local particle parallel velocity $v_\|$ is within 5% of the field-aligned component of the local wave phase velocity $v_{p\|}$. In other words, the particles are initially introduced into the wave at a point in the southern hemisphere (see Figure 1) where $v_\| \geq 1.05 v_p$, and the integration is carried out until a point is reached in the northern hemisphere where $v_\| \geq v_p \pm 0.05 v_p$ or where the wave pulse terminates, whichever comes first. At the termination of the integration (i.e., interaction) each particle has local $v_\|$ and α that correspond to an equatorial pitch angle of $\alpha_{eq} + \Delta\alpha_{eq}$ and parallel velocity of $v_{\|_{eq}} + \Delta v_{\|_{eq}}$. The quantities $\Delta\alpha_{eq}$ and $\Delta v_{\|_{eq}}$ then represent the pitch angle and parallel velocity "scattering" suffered by that particle as a result of its interaction with the wave.

The mean scattering, $\langle\Delta\alpha_{eq}\rangle$ ($\langle\rangle$ denote averaging over the initial phases), of a single sheet of electrons as a function of sheet equatorial parallel velocity is illustrated in Figure 2. The wave intensity $\mathbf{B}_\perp = 10$ pT corresponds to $\mathbf{E}_\| = 15$ μV/m. The solid curve shows the mean final scattering of sheets at the end point of the integration of equations of motion, while the dashed curve represents the mean scattering of sheets at the time they cross the equator. The result shows that the final scattering is, on average, one order of magnitude smaller than the equatorial scattering. The equatorial scattering is negative, i.e., the mean equatorial pitch angle of the 12 test electrons forming a sheet is lowered. To explain the results shown in Figure 2, it is useful to study trajectories of individual electrons.

An expanded view of the electron's parallel velocity and phase behavior during a 400-ms window centered around the first resonance point at $t = 0$ is shown in Figure 3. It can be seen that the phase increases rapidly before the first resonance and the increase slows down as electrons approach the first resonance point, at which the first derivative of phase is zero. After the first resonance, untrapped and trapped electrons execute different phase behavior. Untrapped electrons (Figures 3*a*-3*c*) are associated with a constantly decreasing phase as a result of $v_\| > v_{p\|}$, while trapped electrons (Figure 3*d*) exhibit an oscillatory phase behavior as they oscillate in the wave potential well. Here we consider an electron to be trapped if its phase executes at least one complete oscillation. Figure 3 also illustrates the role of the initial phase angle between an electron and the wave. By comparing the phase behavior of the electrons shown in Figures 3*c* and 3*d*, we see that the difference in their phases at the resonance point ($t = 0$) is less than 5°, but the electron in Figure 3*c* is not trapped, whereas that in Figure 3*d* is trapped.

These four sample trajectories are representative of typical perturbations of electron motion induced by the wave forces. When the energies of all 12 test electrons are added together, the results show that there is an energy increase (average about 2% of the initial total energy) between −4° and 4° latitude, consistent with the result shown in Figure 2. The increase in energy is caused by the acceleration of untrapped electrons such as those shown in Figures 3*a*, 3*b*, and 3*c*, while the energy envelope oscillations are caused by

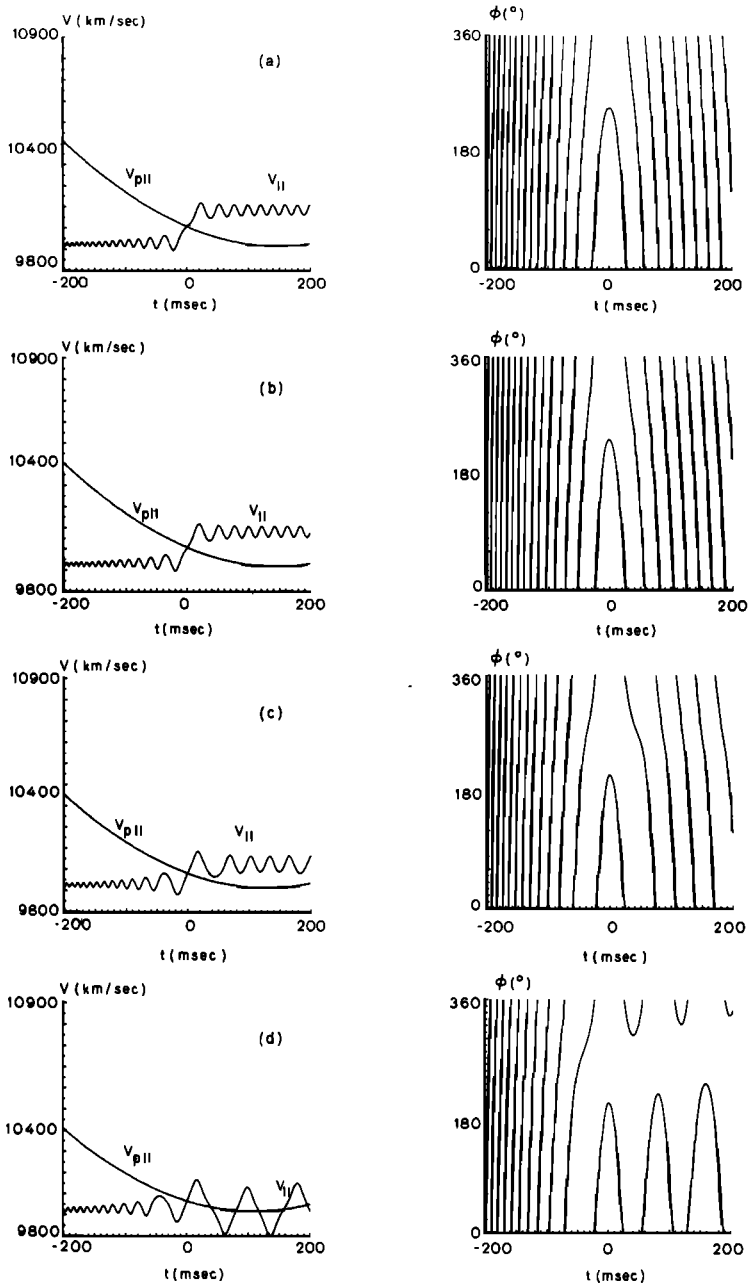

Fig. 3. Single electron trajectories for $B_\perp = 10$ pT. The electron parallel velocity $v_{||}$ and phase ϕ as a function of time. Time $t = 0$ indicates occurrence of the first resonance.

trapped electrons such as that of Figure 3*d*. In the particular example there were seven untrapped electrons and five trapped electrons. Beyond $\lambda = 4°$ the total energy of the sheet returns almost to the initial level. Here we recall that an increase of the electron energy yields a decrease in pitch angle.

The above results suggest that the longitudinal resonance interaction with a monochromatic continuous wave (CW) signal is confined to a relatively small region around the equator. The controlling factor in the interaction that determines the amount of energy exchanged is the variation of phase ϕ which determines whether electrons become trapped in the wave's potential well.

Next we consider the scattering of a single electron sheet interacting with a monochromatic CW wave which is amplified near the equator by some other mechanism such as gyroresonance interaction with counterstreaming electrons. Such amplification of CW waves may take place close to the equator [*Helliwell*, 1967].The length of the growth region is taken to be ~1000 km. The wave amplitude, before it reaches the equatorial growth region, is taken to be 0.1 pT.

Figures 4 and 5 illustrate the scattering of a single sheet as a function of the initial parallel velocity $v_{||eq_0}$. In all computations the wave amplitude is $B_\perp = 10$ pT, or $E_{||} = 15$ μV/m, while the equatorial pitch angle is taken to be 10°, 30°, 50°, and 70°. The total sheet scattering is computed twice for each parallel velocity increment; it is computed once using the complete averaged equations of motion, and again using only the qE term in (2) with $J_o(\eta) = 1$ and $J_1(\eta) = 0$. The latter case represents an electrostatic wave with only a z component and with no transverse phase variation.

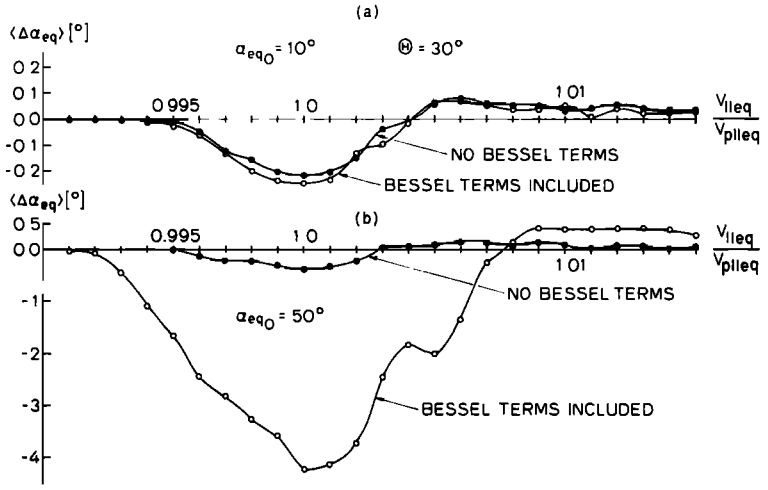

Fig. 4. Mean scattering as a function of parallel velocity. The mean scattering is computed for longitudinal resonance interactions with a CW signal which is amplified after it crosses the equator. The results indicate that the wave magnetic forces become important at larger pitch angles; then it is necessary to include Bessel terms in the equations of motion.

As discussed earlier, the effects of the Bessel terms, i.e., the effects of the wave magnetic field forces, are expected to be significant at larger pitch angles, while at lower pitch angles the error in leaving out these terms is expected to be small [*Inan and Tkalcevic*, 1982]. From Figure 4*a*, for $\alpha_{eq} = 10°$, it is evident that this expectation is confirmed. On the other hand, as the pitch angle increases, the difference between the results becomes much larger, and for $\alpha_{eq} = 70°$ there is almost no scattering if we exclude the Bessel terms from the equations of motion (Figure 5b), whereas the scattering calculated using the complete equations is about $-6°$ at $v_{\|eq} = v_{p\|eq}$. These examples demonstrate that the wave magnetic field forces are important in governing the motion of electrons with high pitch angles.

The dependence of scattering on wave amplitude is depicted in Figure 6. The three different curves shown here represent scattering of sheets with three different initial parallel velocities $v_{\|eq_o}$. A sheet with $v_{\|eq_o} = v_{p\|eq}$ has the optimal parallel velocity as required by the resonance condition. Two other sheets with $v_{\|eq_o} = 0.995 v_{p\|eq}$ and $v_{\|eq_o} = 1.005 v_{p\|eq}$ are slightly off resonance when they encounter the wave growth region at the equator being somewhat slower and faster than the phase front of the wave, respectively. We note from Figure 6 that, as an example, the particle sheet with $v_{\|eq} = v_{p\|eq}$ is scattered about $-0.1°$ when interacting with a relatively weak wave with $B_\perp = 5$ pT. On the other hand, the other two sheets require a wave with $B_\perp = 18$ pT to achieve the same amount of scattering. For $B_\perp < 18$ pT, scattering of the sheet with $v_{\|eq} = 0.995 v_{p\|eq}$ is small and negative, whereas scattering of the sheet with $v_{\|eq} = 1.005 v_{p\|eq}$ is also small, but positive. The direction of energy exchange depends on the relative magnitudes of the parallel and phase velocities. If an electron is faster than a wave, it is decelerated and loses its kinetic energy. If an electron is slower than a wave, it is accelerated and gains kinetic energy. If the parallel velocity of an electron is increased (decreased), its equatorial pitch angle becomes smaller (larger). This explains the behavior of the two sheets with $v_{\|eq_o} = 0.995 v_{p\|eq}$ and $v_{\|eq_o} = 1.005 v_{p\|eq}$ for $B_\perp < 18$ pT. Note here that the sheet with $v_{\|eq_o} = v_{p\|eq}$ does not show similar behavior for $B_\perp > 18$ pT. Careful study of the trajectories of individual test electrons

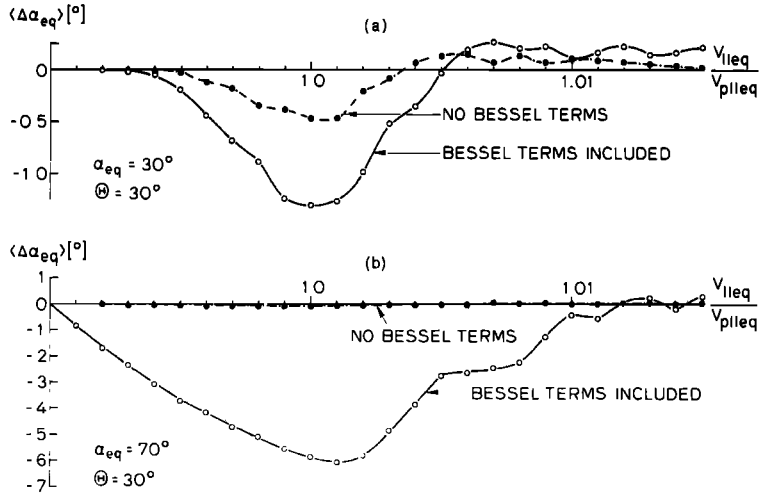

Fig. 5. Mean scattering as a function of parallel velocity. The format is the same as Fig. 4, except that (*a*) $\alpha_{eq} = 30°$, and (*b*) $\alpha_{eq} = 70°$.

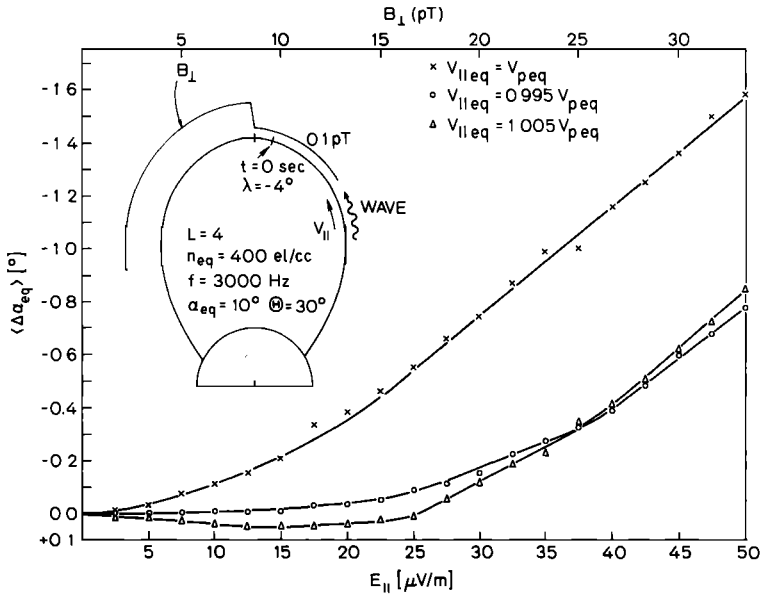

Fig. 6. Mean scattering as a function of wave amplitude for the amplified CW signal. The behavior of the mean scattering indicates the presence of an amplitude threshold effect, i.e., significant scattering is possible only if the wave amplitude exceeds a certain value. The threshold amplitude increases as the absolute difference between the initial parallel and phase velocity becomes larger.

shows that for weak waves all electrons remain untrapped regardless of their initial parallel velocities. As long as the electron parallel velocity does not follow the phase velocity variation, the interaction is generally limited to two relatively small regions around the two resonance points. In the case shown the interactions are further limited to only one side of the equator where the wave amplitude is sufficiently strong. As the wave amplitude increases beyond the equator, the interaction becomes stronger and some electrons become trapped. This transition between the untrapped and trapped mode is characterized by a significant increase in the scattering. The amplitude threshold at which the trapped mode scattering overtakes the untrapped mode scattering depends on the initial parallel velocity $v_{p_{\|}eq_o}$, as shown in Figure 6. The threshold amplitude for $v_{eq_o} = v_{p_{\|}eq}$ is as low as $B_\perp = 3$ pT, with a relatively smooth transition between the two interaction regimes. The amplitude threshold in the two other cases is $B_\perp \simeq 18$ pT with a much sharper transition between two regimes.

Some individual particle trajectories corresponding to the cases described in Figure 6 are illustrated in Figures 7 and 8. Figure 7 shows parallel velocities and phases of four electrons with $v_{\|eq_o} = v_{p_{\|}eq}$, $\alpha = 10°$, and different initial phases ϕ_o, as functions of latitude and time, respectively. The wave amplitude is taken to be $B_\perp = 10$ pT. As in the case for a CW signal, the parallel velocity variation of those electrons is controlled by the initial phase ϕ. For example, the electron trajectory of Figure 7*a* indicates absence of trapping because of an improper phase, whereas the number of oscillations for trapped electrons in the other three cases also depends on the phase at the moment when the parallel velocity equals the wave phase velocity. Figure 8 depicts a time-expanded view of the electron trajectories around the first resonance point. In Figure 8 the time $t = 0$ indicates the first resonance where $v_{\|} = v_{p_{\|}}$. The phase at this point is important in determining the further motion of particles. For example, the phase of the electron shown in Figure 8*a* is such that it is initially strongly decelerated and by the time of phase reversal, i.e., electron acceleration, $v_{\|}$ and $v_{p_{\|}}$ are too different for trapping to be possible. Observing the phase of the electron in Figure 8*b* at $t = 0$, we find it to be significantly smaller than the phase in Figure 8*a*. Because of the difference in phase the deceleration suffered by this second electron is smaller, and eventually the particle becomes trapped and executes one oscillation at the bottom of the potential well. For the next two electrons shown in Figures 8*c* and 8*d* the phases at $t = 0$ are even smaller, resulting in an increasing number of oscillations. We note that the amplitudes of both velocity and phase oscillations decrease as the phase at $t = 0$ decreases. In the example shown in Figure 8*d* the phase at $t = 0$ is very close to the optimal 90° which then results in the strongest trapping. As discussed earlier the 90° phase indicates that an electron is exactly at the bottom of the potential well.

Figure 9 shows the scattering of individual electrons as a function of their initial phases ϕ_o for three different wave amplitudes. This figure confirms the importance of phase as a controlling factor in the longitudinal resonance interaction.

Next we determine the dependence of the scattering efficiency on the wave normal angle. Figure 10 shows $\langle \Delta\alpha_{eq} \rangle$ as a function of θ for $B_\perp = 10$ pT, $\alpha_{eq} = 10°$, and $v_{\|eq_o} = v_{p_{\|}eq}$. The wave function corresponds to that shown in Figure 6. Also shown are the average initial and final energy of the sheet, $\langle E_o \rangle$ and $\langle E_S \rangle$, where $\langle\rangle$ represent averaging over the particles in a given sheet. As noted earlier, the main effect of the wave normal angle increase is an increase of $E_{\|}$. Thus, as the wave normal angle increases, the longitudinal interactions become more effective, as indicated in Figure 10. Furthermore, when the wave normal approaches the resonance cone, electrons are scattered by as much as $-5.5°$, and the sheet energy is increased about 5 times.

Figure 11 shows $\langle \Delta\alpha_{eq} \rangle$ versus $v_{\|}$, and $\langle \Delta E \rangle$ versus $v_{\|}$ for interactions taking place inside and outside the plasmapause

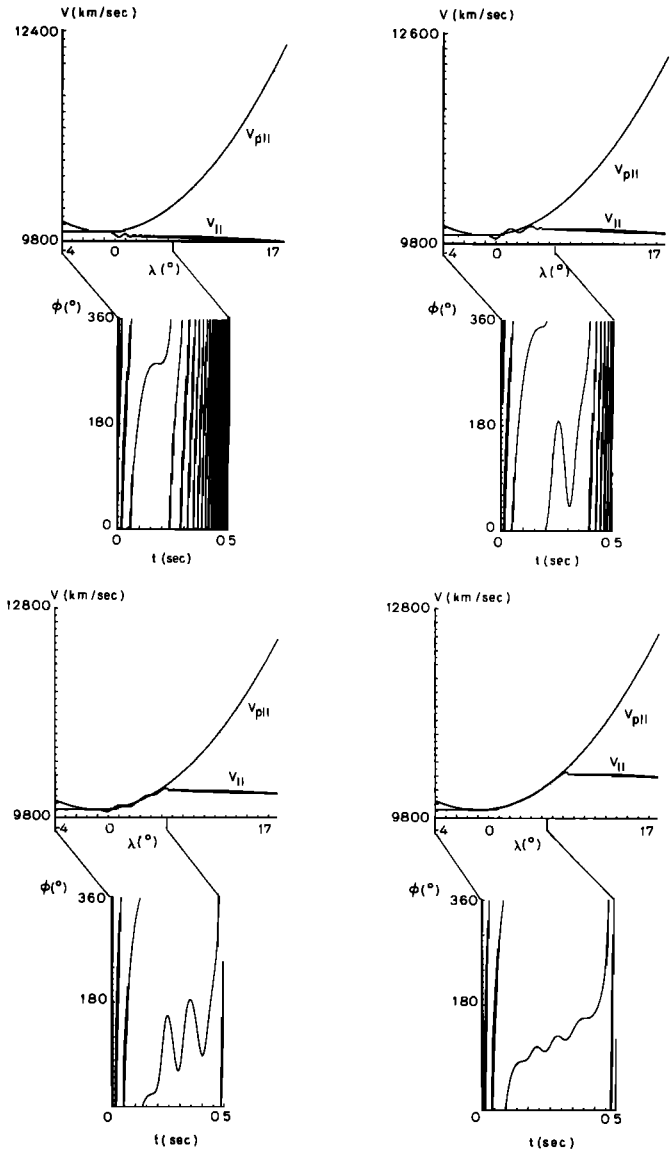

Fig. 7. Single electron trajectories for $B_\perp = 10$ pT. Parallel velocity and phase behavior for electrons with $v_{\parallel eq} = v_{peq}$ and $\alpha = 10^\circ$ interacting with variable amplitude CW signal. The initial electron phase is (*a*) 0°, (*b*) 120°, (*c*) 150°, and (*d*) 300°.

as characterized by different values of the cold plasma density n_{eq}. These results clearly show that interactions outside the plasmapause result in less scattering, but in more energy exchange, than those interactions inside the plasmapause. This result is partly due to the fact that the electric field component of a 10-pT wave is larger in the lower density region [*Tkalcevic*, 1982]. Another factor that plays a role is the fact that for smaller n_{eq} the wave phase velocity is larger and the parallel resonant energy is higher. Higher energy electrons move faster through the wave, and hence the time available for scattering is reduced. Note that although the resonant energy is about 288 eV for $n_{eq} = 400$ el/cm^3, it is 11,529 eV for $n_{eq} = 10$ el/cm^3. Because of this difference in resonant energies, even a relatively small scattering outside the plasmapause results in absolute energy changes that are larger compared to those found inside the plasmapause. Note, however, that the percentage energy change $(\Delta E/E)$ is larger in the higher density region.

This concludes our discussion of single sheet scattering interacting with a one-sided wave function. In the next section we present results involving single sheet scattering in the case of a spatially limited wave distribution.

5. Interaction With a Wave Pulse

In this section we examine the scattering of a single electron sheet as it moves through a wave structure with spatially limited amplitude distribution. Such a distribution may result from a particular configuration of nonducted ray paths or may be due to a wave pulse with finite duration. As depicted in Figure 12*a* the wave signal is taken to have uniform intensity between $\lambda = -10^\circ$ and $\lambda = -7^\circ$, which is equivalent to 1000 km in length. Other interaction parameters are also specified in Figure 12*a*. The interaction is studied for a wide range of initial parallel velocities, $\Delta v_\parallel$, as illustrated in Figure 12*b*. The minimum parallel velocity increment is $0.001 v_{p\parallel eq}$. The wave amplitude is assumed to be zero everywhere except for $-10^\circ < \lambda < -7^\circ$. The

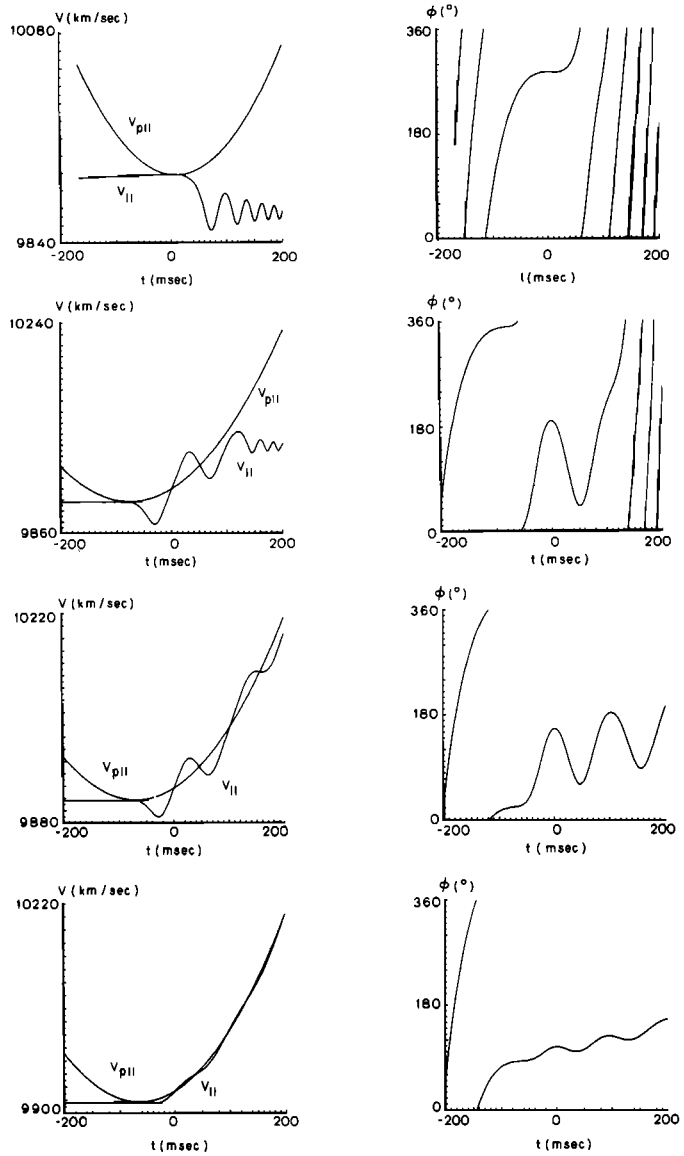

Fig. 8. Single electron trajectories for $B_{\perp} = 10$ pT. Shown here are the parallel velocity and phase variations around the first resonance point at $t = 0$. Other parameters are the same as those in Fig. 7.

scattering results are shown in Figure 13. We explain these results as follows: when the initial parallel velocity is small, for example $v_{||eq}$, the first resonance point is close to the equator. Hence as these electrons travel up the field line toward the equator, they encounter the spatial amplitude pulse, but the electron parallel and wave phase velocities are rather different, resulting in a very weak interaction. As the initial parallel velocity of a sheet is increased, the first resonance point moves away from the equator and closer to the amplitude pulse. The two velocities are then better matched, resulting in a stronger interaction and a negative scattering $\langle \Delta\alpha_{eq} \rangle$. A negative sign of $\langle \Delta\alpha_{eq} \rangle$ means that electrons are accelerated. This acceleration is consistent with the relative ratio of two velocities; namely, before electrons reach the first resonance point their velocity is less than the wave phase velocity, in which case electrons are accelerated in order to match the phase velocity. However, further increase of the parallel velocity beyond $1.082v_{p||eq}$ results in a change of sign of the effective scattering. This occurs when the first resonance point falls within approxi-

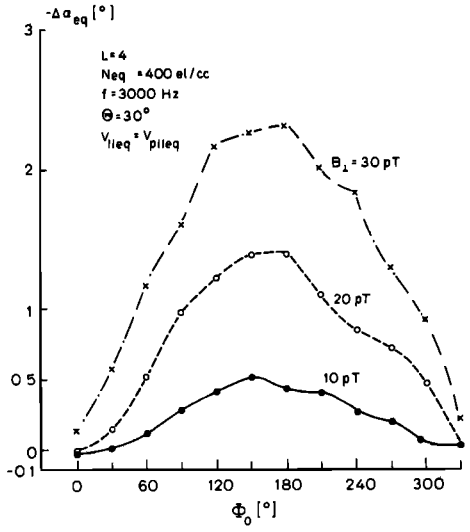

Fig. 9. Total scattering $\Delta\alpha_{eq}$ versus initial phase for different wave amplitudes. The initial pitch angle is $\alpha_{eq} = 10°$.

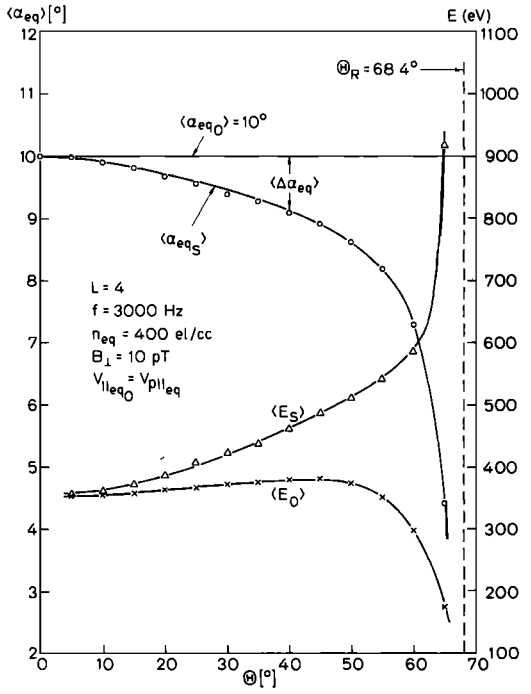

Fig. 10. Mean scattering as a function of wave normal angle. The difference $\langle E_s \rangle - \langle E_o \rangle$ represents the amount of energy gained by electrons.

mately ±0.5° of the pulse front edge at −10°. The principal difference is that electrons become trapped as they interact with the pulse, whereas for lower parallel velocities there were no trapped electrons. When trapping takes place, the parallel velocity follows the phase velocity, which decreases as electrons approach the equator, and this results in a positive sign of scattering $\langle \Delta\alpha_{eq} \rangle$ in Figure 13. Furthermore, as the parallel velocity is increased beyond $1.094 v_{p_{\|}eq}$, the first resonance moves even farther down the field line and interactions become small again. The shaded area in Figure 12*b* indicates the trapping velocity bandwidth $\Delta v_{\|t}$, which is also indicated in Figure 13. When comparing areas of positive and negative scattering in Figure 13, they turn out to be approximately the same, which means that the net energy exchange is small.

This example is a good illustration of the different features of the longitudinal resonance interaction. We see that the electron behavior is very dissimilar in cases with and without trapping. Untrapped electrons change their velocity depending on the ratio of phase and parallel velocities, while the trapped electrons travel along together with their parallel velocity following the wave phase velocity. This means that the number density of trapped electrons will build up as more and more electrons fall into the trap. It has been suggested that this trapping mechanism might account for the production of whistler precursors [*Park and Helliwell*, 1977]. In this process a strong whistler, whose $E_{\|}$ exceeds the trapping threshold (~25 μV/m in Figure 6), traps longitudinally resonant electrons as the whistler travels toward the equator. An increase in the number density of up to a factor of 2 has been estimated for this process [*Tkalcevic*, 1982]. When this temporary enhancement of particle flux reaches the equator, it causes the threshold for emission triggering [*Helliwell et al.*, 1980] to drop below the level of available triggering signals, such as power line radiation. Cyclotron emissions are then triggered in the backward direction, arriving at the receiver ahead of the two-hop of the whistler. An intensity threshold for the onset of precursors has been found in the data, giving support to this hypothesis [*Tkalcevic*, 1982]. The same basic mechanism has been advanced to explain an association between VLF chorus and electrostatic emissions observed is the terrestrial [*Reinleitner et al.*, 1984] as well as Jovian and Saturnian magnetospheres.

Figure 14 illustrates the same type of interaction except that the spatial amplitude pulse is on the other side of the equator. The corresponding scattering results are shown in Figure 15. These results may be explained using the same analysis as that employed in the previous example. Trapping occurs when the first resonance point is close to the pulse front edge at $\lambda = 7°$, although the trapped electron scattering is now negative as the phase velocity increases. The untrapped particle scattering is positive because the phase velocity is smaller than the parallel velocity before the resonance point is reached.

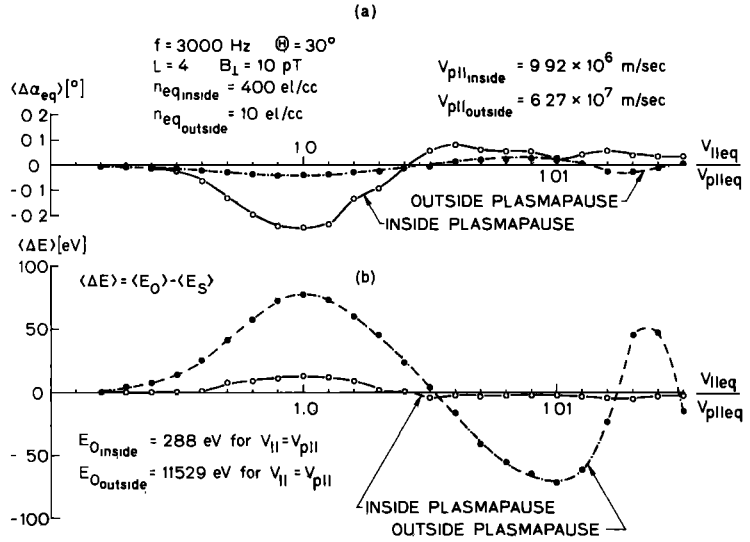

Fig. 11. Comparison between the effects of longitudinal resonance interactions inside and outside the plasmapause. (*a*) The mean scattering $\langle \alpha_{eq} \rangle$. (*b*) The corresponding energy exchange $\langle \Delta E \rangle$.

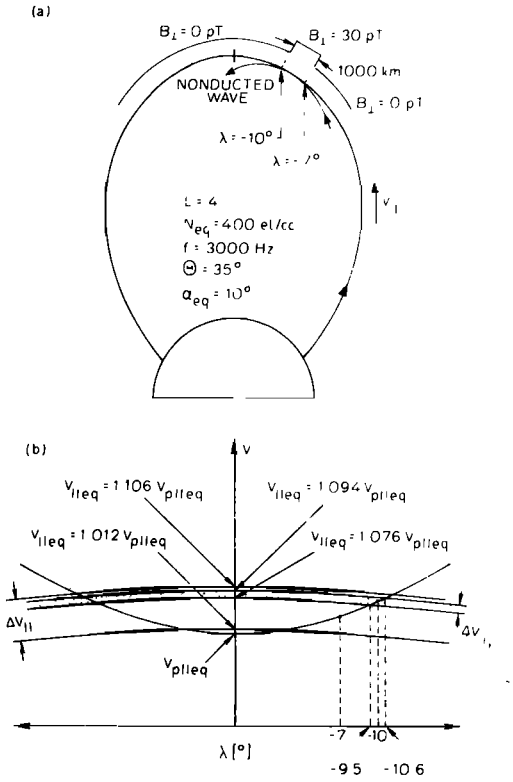

Fig. 12. Interaction with spatial amplitude pulse extending between $\lambda = -10°$ and $\lambda = -7°$. (*a*) The position of spatial pulse on the field line. (*b*) The range of affected initial parallel velocities.

6. Interaction With a Full Distribution of Particles

In the previous sections we have presented results on pitch scattering of single test particles. The purpose of that analysis was to clarify various aspects of the longitudinal resonance process. In this section we carry those calculations one step further by increasing the number of test electrons in order to simulate a full distribution for the purpose of computing the wave-induced precipitation flux.

For the cases presented here we assume interactions with a one-sided wave function. As was discussed earlier, the wave-induced scattering for that type of wave function is found to be larger than would result from interaction with continuous wave signals.

The energetic electron population is described in terms of an equatorial distribution function $f_{eq}(v_{\|eq}, \alpha_{eq})$. From this point on we drop the subscript "eq" and all quantities represent equatorial values unless specified otherwise. The distribution function is given in $v_\| - \alpha$ space because it is a convenient representation which directly shows the pitch angle scattering $\Delta\alpha$ and it is easy to determine a normalized velocity $v_\|/v_{p_\|}$ which is one of the prime factors affecting the interaction process. The velocity space volume element is then given as $v_\|^2 \frac{\sin\alpha}{\cos^3\alpha} d\alpha dv_\| d\phi$ [*Inan et al.*, 1978].

Now we recall results of Figures 4 and 5 showing the mean scattering of a single sheet as a function of the sheet initial parallel velocity. From these it is evident that the trapping velocity range considered is limited to a narrow strip around $v_\| = v_{p_\|}$, while the pitch angle range extends from α_{lc} to α_{max}. The value of α_{max} may be as large as 90°, although in our model we employ a slightly lower value because of the time-averaged nature of the equations of motion. The angle $\alpha_{lc} = 5.5°$ is the nominal loss cone angle for the dipole field line $L = 4$ [*Inan et al.*, 1978]. As already shown in Figures 4 and 5, the trapping velocity bandwidth increases with increasing pitch angle due to the effects of the wave magnetic field forces. For the parameters used here the trapping velocity bandwidth $\Delta v_{\|t}$ is $\sim 0.4\%$ of $v_{p_\|eq}$ for $\alpha = 10°$, and $\sim 1\%$ of $v_{p_\|eq}$ for $\alpha = 70°$. Again, it should be noted that this velocity bandwidth refers to the trapped electrons only. The untrapped electrons have quite different behavior; if the initial parallel velocity is smaller than the lower trapping velocity limit, the scattering is negligible because the $v_{p_\|}$ and the $v_\|$ are never matched along the field line. On the other hand, if the initial parallel velocity of an untrapped electron is larger than the upper trapping

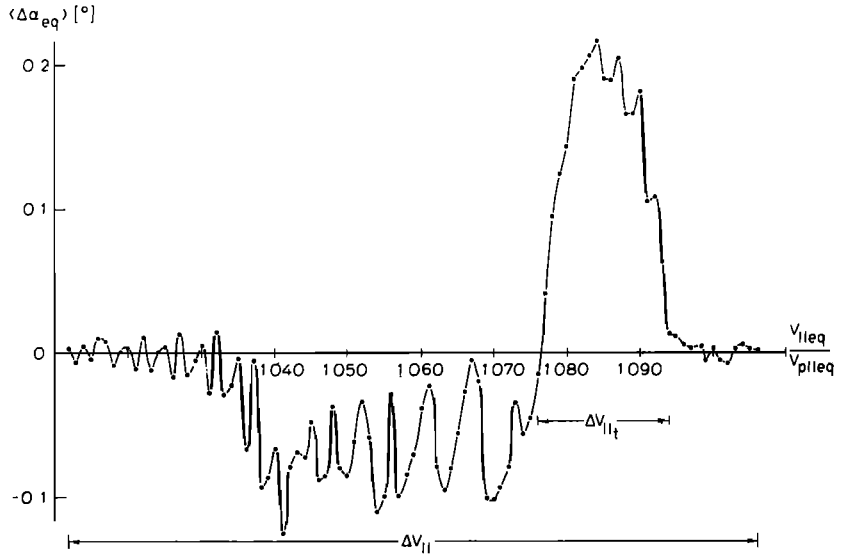

Fig. 13. Mean scattering for interactions with a spatial amplitude pulse extending between $\lambda = -10°$ and $\lambda = -7°$. Electrons with initial velocities within the $\Delta v_{\|_t}$ range are trapped, while electrons with other initial parallel velocities remain untrapped.

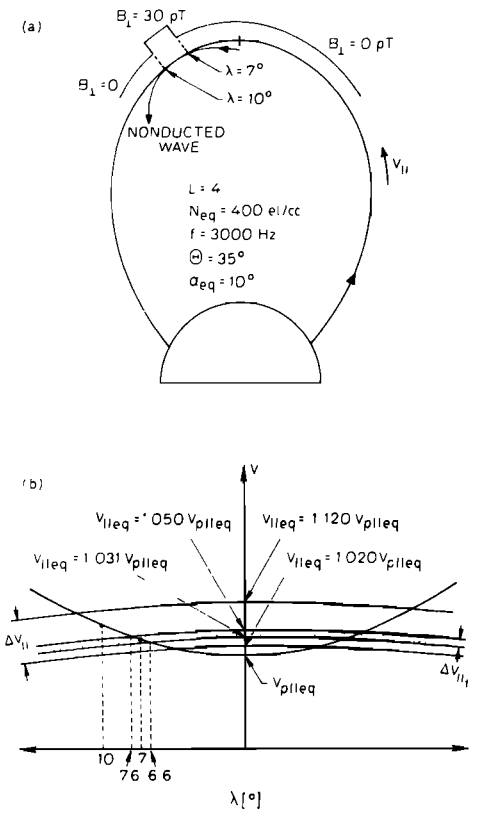

Fig. 14. Interaction with spatial amplitude pulse extending between $\lambda = 7^\circ$ and $\lambda = 10^\circ$. The format is the same as that of Fig. 13.

velocity limit, there are always two resonances; scattering at the first resonance is negligible because the wave amplitude is very small, whereas at the second resonance point, where $v_{||}$ exceeds $v_{p_{||}}$, the untrapped electrons are decelerated. The above mentioned different classes of electrons are illustrated in Figure 16. The scattering of untrapped electrons is much smaller than it is for the trapped electrons, but the interaction velocity range for untrapped electrons is larger than the trapping velocity bandwidth. The effects of trapped and untrapped electrons on the wave amplitude are exactly opposite; the trapped electrons are accelerated and derive energy from the wave, whereas the untrapped electrons are decelerated and give energy to the wave. This behavior of trapped and untrapped particles is similar to that in the case of first-order gyroresonance interaction involving longitudinally ($\mathbf{k} \parallel \mathbf{B}_o$) propagating waves [*Bell and Inan*, 1981].

As illustrated in Figure 16, we consider a region in $v_{||} - \alpha$ space (cross-shaded) containing electrons that are effectively scattered into the loss cone. Here the determination of α_{max} is based on the maximum expected scattering under given conditions. This region in the $v_{||} - \alpha$ space is further divided into a number of mesh points identified by their $v_{||}$ and α, and this mesh then represents the initial distribution. The number of electrons at each mesh point is equal to 12, reflecting the fact that electrons are uniformly distributed in phase. Figure 17*a* illustrates the unperturbed distribution function; note that we use the number density of electrons N_e rather than $f(v_{||}, \alpha)$. The number density and $f(v_{||}, \alpha)$ are related through [*Inan et al.*,1978]

$$N_e = 2\pi f(v_{||}, \alpha) v_{||}^2 \frac{\sin \alpha}{\cos^3 \alpha} \Delta v_{||} \Delta \alpha \qquad (6)$$

Using (6) it is also possible to find the actual number of electrons represented by a single test electron.

During the interaction the initial distribution of electrons (Figure 17*a*) is perturbed by the wave, and the final distribution shown in Figure 17*b* is obtained. Note that the velocity mesh size is different in Figures 17*a* and 17*b*, since the energy of the electrons tends to be significantly increased during the interaction. In addition to an overall increase in electron energy, three fast electrons are seen to scatter into the loss cone. In the next section we estimate the wave-induced precipitation fluxes for three particular cases.

7. WAVE-INDUCED PRECIPITATION FLUX

Here we compute the precipitated electron fluxes involving a one-sided wave function and for three different maximum wave intensities ($E_{||} = 50$, 150, and 250 μV/m). The maximum initial pitch angle α_{max} considered in these calcu-

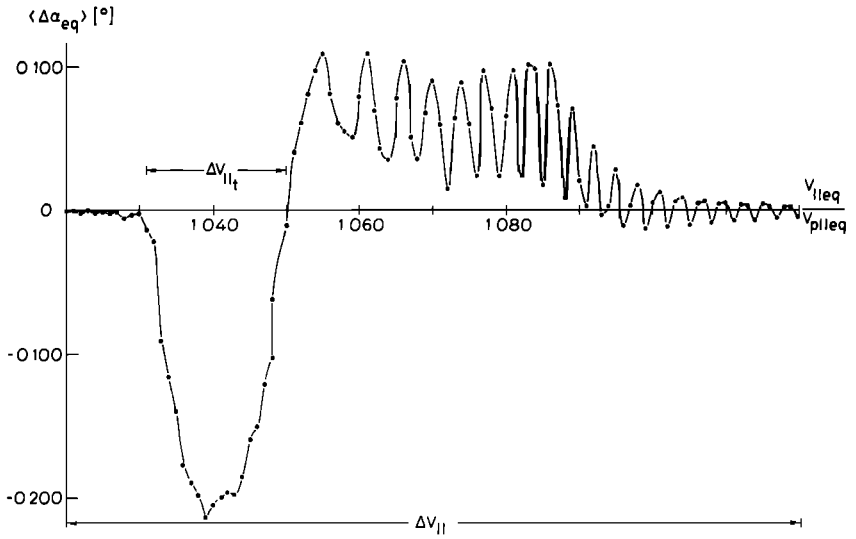

Fig. 15. Mean scattering for interactions with a spatial amplitude pulse extending between $\lambda = 7^\circ$ and $\lambda = 10^\circ$. Only electrons with $v_{||}$ in the $\Delta v_{||_t}$ range are trapped.

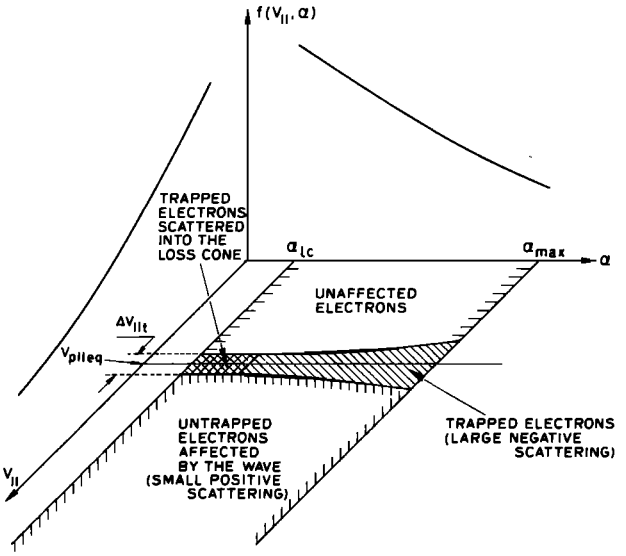

Fig. 16. General distribution function. Differently shaded areas indicate the various behavior of electrons as they interact with the variable amplitude wave.

lations is 10°, since there are no electrons with $\alpha > 10°$ that can be scattered into the loss cone even for the largest $E_{\parallel}$ considered. The initial unperturbed number density function is the same in all three examples and was already shown in Figure 17*a*. Furthermore, the particle distribution function is taken to be

$$f(v,\alpha) = \frac{A}{v^4} g(\alpha) \tag{7}$$

where A is a constant and $g(\alpha)$ is some function of pitch angle. In our calculations, $g(\alpha)$ is assumed to be an isotropic function given by

$$g(\alpha) = \begin{cases} 1 & \alpha > \alpha_{lc} \\ 0 & \alpha < \alpha_{lc} \end{cases} \tag{8}$$

The following analysis is similar to that presented by *Inan et al.* [1978], where pitch angle scattering due to gyroresonance was studied. We first determine the wave-induced perturbations of the pitch angle distribution $f(\alpha)$ as obtained by integrating $f(v_{\parallel},\alpha)$ over the velocity range of interest. In the cases considered here, for a 5-kHz wave it is found that the maximum parallel velocity after the interaction is $v_{\parallel max} = 1.8 v_{p_{\parallel}}$, whereas the minimum parallel velocity is $v_{\parallel min} = 0.98 v_{p_{\parallel}}$. The equatorial phase velocity $v_{p_{\parallel}}$ for a 5-kHz wave is 11.23×10^6 m/s. Thus the pitch angle distribution is given by

$$f(\alpha) = 2\pi \int_{0.98 v_{p_{\parallel}}}^{1.8 v_{p_{\parallel}}} f(v_{\parallel},\alpha) v_{\parallel}^2 dv_{\parallel} \tag{9}$$

remembering that electrons are uniformly distributed in initial phase, which accounts for the factor 2π in (9).

Figure 18 shows the normalized pitch angle distribution $f(\alpha)$ as a function of α for different wave intensities. The dashed curves show the initial unperturbed distributions, whereas the solid curves indicate the final distributions. These results show that the longitudinal resonance interaction requires rather strong waves in order to scatter electrons into the loss cone. For a wave with $E_{\parallel} = 50\ \mu$V/m ($B_{\perp} = 14$ pT) the perturbations are very small, and only a few electrons are scattered below α_{lc}. When the wave amplitude is increased, the loss cone starts to fill with electrons, and also electrons with higher pitch angles are scattered down to lower pitch angles. This process is best illustrated in the case of a 250 μV/m wave, where the loss cone is filled with electrons having a wider range of initial pitch angles than the electrons reaching the loss cone in the two other cases.

The total number density of electrons precipitated in the velocity range 0.98 $\frac{1}{N}$ to $1.8 v_{p_{\parallel}}$ is given by

$$N = 2\pi \int_0^{\alpha_{lc}} \int_{0.98 v_{p_{\parallel}}}^{1.8 v_{p_{\parallel}}} f(v_{\parallel},\alpha) v_{\parallel}^2 \frac{\sin\alpha}{\cos^3\alpha} dv_{\parallel} d\alpha L^3 (1+3\sin^2\lambda)^{1/2} \tag{10}$$

where the factor $L^3(1+3\sin^2\lambda)^{1/2}$ accounts for the convergence of the field line going from the equator to ionospheric heights. The precipitated energy deposition rate is computed in similar fashion by including the energy weighting factor $\frac{1}{2} m \frac{v_{\parallel}^2}{\cos^2\alpha}$ in (10) which then yields

$$Q = 2\pi \int_0^{\alpha_{lc}} \int_{0.98 v_{p_{\parallel}}}^{1.8 v_{p_{\parallel}}} f(v_{\parallel},\alpha) v_{\parallel}^2 \frac{\sin\alpha}{\cos^3\alpha} \frac{1}{2} m \frac{v_{\parallel}^2}{\cos^2\alpha} v_{\parallel} dv_{\parallel} d\alpha L^3 (1+3\sin^2\lambda)^{1/2} \tag{11}$$

The integrals in (10) and (11) are easily evaluated by numerical integration. For the three examples considered, the normalized energy deposition rates, defined as $Q_N = Q/A$ where A is defined in (7) are

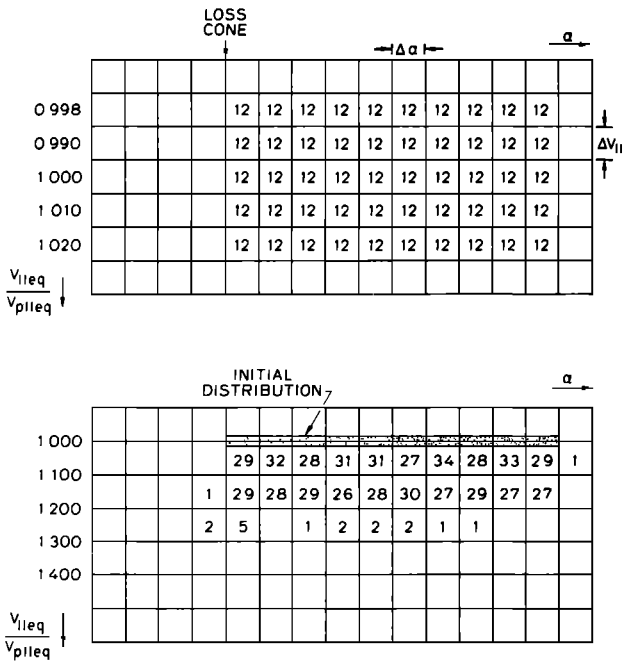

Fig. 17. Simulation of the distribution function. (*a*) The unperturbed distribution. (*b*) Perturbed distribution. The numbers in each individual cell indicate the number density of electrons.

$E_{\parallel}(\mu V/m)$	Q_N
50	0.96×10^{-14}
150	0.81×10^{-12}
250	0.35×10^{-11}

To compute the total energy deposition, it is necessary to evaluate the constant A. This can be done by computing the total number density N_e in electrons per cubic centimeter in the specific velocity range 0.98-1.8 $v_{p_{\parallel}}$. In this case,

$$N_e = 2\pi \int_0^{\pi} \int_{0.98v_{p_{\parallel}}}^{1.8v_{p_{\parallel}}} \frac{A}{v^4} v^2 \sin\alpha dv d\alpha \qquad (12)$$

The above integral yields

$$A = 2 \times 10^8 N_e \qquad (13)$$

Finally, to determine typical values of A, we use data from reported measurements of N_e. From *Schield and Frank* [1970] we find that $N \simeq 1$ el/cm^3 in the 1–2 keV range and that the number density varies as v^{-4} where v is the particle velocity. In our case the electron energies are 300–1000 eV which results in $N_e = 10$ el/cm^3, since the number density increases with decreasing electron energy. Substituting $N_e = 10$ el/cm^3 in (13), we find $A = 2 \times 10^9$.

Using this value for A, the precipitated energy deposition rates are found to be

$E_{\parallel}(\mu V/m)$	$Q(ergs/cm^2)$
50	1.94×10^{-5}
150	1.66×10^{-3}
250	$7\,40 \times 10^{-3}$

The above values represent the flux precipitated by a 5-kHz wave, having a one-sided wave intensity distribution, from an initial distribution of energetic particles given by (7) and (8). These flux levels are much smaller than those expected under similar conditions from gyroresonant wave-particle interactions [*Inan et al.*, 1978], where flux levels of 0.01–0.2 erg/cm^{2}s would be expected for a 10-pT wave. Note that 10 pT of perpendicular wave magnetic field intensity corresponds to $E_{\parallel} = 30\mu$V/m for $\theta = 30°$ and $f = 5$ kHz, at the equator. For the parameters considered here, the difference between the two cases is almost three orders of magnitude.

8. Conclusions

In conclusion, we summarize our results as follows:

1.) Using the time-averaged nonlinear equations of motion in computing the nonlinear trajectories of electrons interacting in the Landau resonance made with whistler mode signals propagating obliquely in an inhomogeneous medium, it was confirmed that the effects of wave magnetic forces can be neglected for low pitch angles, high wave normal angles, and/or high normalized wave frequency as predicted by *Inan and Tkalcevic* [1982]. It was also shown that at higher pitch angles the wave magnetic field forces become significant and must be included for a correct formulation of the problem.

2.) Our test particle results distinguished between two classes of electrons on the basis of the variation of their phases with respect to the wave. In a case where the phase variation is bounded, i.e., remains less than 2π, the electron is said to be trapped, whereas unbounded phase variation characterizes the untrapped electrons. The scattering and corresponding energy exchange for the trapped and untrapped electrons exhibit significantly different characteristics.

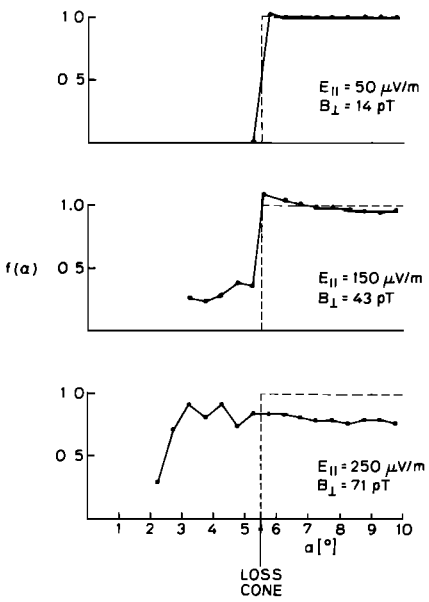

Fig. 18. Normalized electron distribution $f(\alpha)$. The dashed lines represent the unperturbed distribution. The solid curves represent the perturbed distribution.

3. It is also found that the trapping of electrons is easier under conditions of spatial amplitude variation of a narrowband signal rather than for a constant amplitude. Results were presented for a constant amplitude continuous wave signal, a continuous wave signal amplified at the equator through some other mechanism (e.g., gyroresonance), and also for a pulse with a spatially limited amplitude distribution that might be established as a result of a particular distribution of nonducted ray paths in the magnetosphere.

4. It is also shown that the longitudinal resonance process involves a wave amplitude threshold effect, i.e., the trapping of electrons is possible only if the amplitude of the wave parallel electric field $E_{\parallel}$ exceeds a certain value. The trapped electrons also become space bunched and temporarily increase the electron density over a particular range of parallel velocities. Such a density enhancement may play a role in the triggering of gyroresonance emissions, such as whistler precursors [*Park and Helliwell*, 1977; *Tkalcevic*, 1982]. This same basic mechanism has also been advanced to explain an association between VLF chorus and electrostatic bursts observed in the terrestrial as well as Jovian and Saturnian magnetospheres [*Reinleitner et al.*, 1984].

5. The full distribution results show that the precipitation expected from longitudinal resonance scattering is small compared to gyroresonance-induced precipitation for waves of comparable amplitude. At $L = 4$ and for the parameters considered here the scattering efficiencies of the two processes may differ by as much as three orders of magnitude under similar conditions.

Acknowledgments. We thank our colleagues in the STAR Laboratory for many valuable discussions. This research was supported in part by NASA under grant NGL-05-020-008, and in part by the

Division of Atmospheric Sciences of the National Science Foundation under grant ATM80-18248. Much of the computer modeling was done by remote job entry using the facilities of the National Center for Atmospheric Research which is sponsored by the National Science Foundation. The typescript was prepared by G. Walker and N. Leger.

The Editor thanks the referee for assistance in evaluating this paper.

REFERENCES

Angerami, J. J. and J. O. Thomas, Studies of planetary atmospheres, 1, The distribution of electrons and ions in the earth's exosphere, *J. Geophys. Res., 69*, 4537, 1964.

Budden, J. G., Radio waves in the ionosphere, Cambridge University Press, New York, 1961.

Cuperman, S., and A. Sternlieb, Obliquely propagating unstable whistler waves: a computer simulation, *J. of Plasma Physics, 11*, 175, 1974.

Gendrin, R., Le guidage des whistlers par le champ magnetique, *Planet. Space Sci., 5*, 274, 1961.

Helliwell, R. A., A theory of discrete VLF emissions from the magnetosphere, *J. Geophys. Res., 72 (19)*, 4773, 1967.

Helliwell, R. A., D. L. Carpenter, and T. R. Miller, Power threshold for growth of coherent VLF signals in the magnetosphere, *J. Geophys. Res., 85*, 3360, 1980.

Inan, U. S., and T. F. Bell, The plasmapause as a VLF wave guide, *J. Geophys. Res., 82(19)*, 2819, 1977.

Inan, U. S., Nonlinear gyroresonant interactions of energetic particles and coherent VLF waves in the magnetosphere, Tech. Report No. 3414-3, Radioscience Lab., Stanford Electronics Labs, Stanford, CA 1977.

Inan, U. S., T. F. Bell, and R. A. Helliwell, Nonlinear pitch angle scattering of energetic electrons by coherent VLF waves in the magnetosphere, *J. Geophys. Res., (A7) 83*, 3235, 1978.

Inan, U. S., and S. Tkalcevic, Nonlinear equations of motion for Landau resonance interactions with a whistler mode wave, *J. Geophys. Res., 87*, 2363, 1982.

Jorgensen, T. S., Interpretation of auroral hiss measured on OGO 2 and at Byrd station in terms of incoherent Cerenkov radiation, *J. Geophys. Res., 73*, 1055, 1968.

Maggs, J. E., Coherent generation of VLF hiss, *J. Geophys. Res., 81*, 1707, 1976.

Nunn, D., Wave particle interaction in electroptatic waves in an inhomogeneous medium, *Planet. Space Sci., 6*, 291, 1971.

Nunn, D., The sideband instability of electrostatic waves in an homogeneous medium, *Planet. Space Sci., 21*, 67, 1973.

Park,C. G., and R. A. Helliwell, Whistler precursors: A possible catalytic role of power line radiation, *J. Geophys. Res., 82*, 3634, 1977.

Reinleitner, L. A., D. A. Gurnett, and D. L. Gallagher, Chorus-related electrostatic bursts in the earth's outer magnetosphere, *Nature, 295*, 46, 1982.

Reinleitner, L. A., D. A. Gurnett, and T. E. Eastman, Electrostatic bursts generated by electrons in Landau resonance with whistler mode chorus, *J. Geophys. Res., 88*, 3079, 1983.

Reinleitner, L. A., W. S. Kurth, and D. A. Gurnett, Chorus-related electrostatic bursts at Jupiter and Saturn, *J. Geophys. Res., 89*, 75, 1984.

Schield, M. A., and L. A. Frank, Electron observations between the inner edge of the plasma sheet and the plasmasphere, *J. Geophys. Res., 75*, 5401, 1970.

Swift, D. W., and J. R. Kan, A theory of auroral hiss and implications on the origin of auroral electrons, *J. Geophys. Res., 80*, 985, 1975.

Thorne, R. M., E. J. Smith, R. K. Burton, and R. E. Holzer, Plasmaspheric hiss, *J. Geophys. Res., 78*, 1581, 1973.

Tkalcevic, S., Nonlinear longitudinal resonance interaction of energetic charged particles and VLF waves in the magnetosphere, *Tech. Rep. E4-2311*, Radiosci. Lab., Stanford Electr. Labs, Stanford Univ., Stanford, Calif., 1982.

R. A. Helliwell, U. S. Inan, and S. Tkalcevic, Space, Telecommunications, and Radioscience Laboratory, Stanford University, CA 94305.

(Received March 26, 1984;
revised July 11, 1984;
accepted July 23, 1984.)